Estuarine, Coastal and Shelf Science 95 (2011) 298–306

Contents lists available at SciVerse ScienceDirect

Estuarine, Coastal and Shelf Science

journal homepage: www.elsevier.com/locate/ecss

High-frequency turbulence and suspended sediment concentration measurements in the Garonne River tidal bore

Hubert Chanson[a,*], David Reungoat[b], Bruno Simon[a,b], Pierre Lubin[b]

[a] The University of Queensland, School of Civil Engineering, Brisbane QLD 4072, Australia
[b] Université de Bordeaux, I2M, 16 avenue Pey-Berland, CNRS UMR 5295, Pessac, France

ARTICLE INFO

Article history:
Received 14 January 2011
Accepted 15 September 2011
Available online 22 September 2011

Keywords:
tidal bore
Garonne River
field works
turbulence
suspended sediment concentration
suspended sediment flux
sediment processes

ABSTRACT

The study details new sediment concentration measurements associated with some turbulence characterisation conducted at high-frequency in the undular tidal bore of the Garonne River (France). Acoustic Doppler velocimetry was used, and the suspended sediment concentration was deduced from the acoustic backscatter intensity. The field data set demonstrated some unique flow features of the tidal bore including some large and rapid turbulent velocity fluctuations during and after the bore passage. Some unusually high suspended sediment concentration was observed about 100 s after the tidal bore front lasting for more than 10 min. It is thought that the tidal bore passage scoured the bed and convected upwards the bed material, reaching the free-surface after the bore passage. Behind the tidal bore, the net sediment flux magnitude was 30 times larger than the ebb tide net flux and directed upstream. A striking feature of the data set was the intense mixing and suspended sediment motion during the tidal bore and following flood tide. This feature has been rarely documented.

1. Introduction

A tidal bore is a series of waves propagating upstream as the tidal flow turns to rising, forming during spring tide conditions when the tidal range exceeds 4–6 m and the flood tide is confined to a narrow funnelled estuary whose bathymetry amplifies the tidal wave. During the flood tide when the sea level rises with time, the tidal wave propagates upstream and becomes steeper until it forms a bore front. The inception, development and propagation of the tidal bore may be predicted using the method of characteristics (Henderson, 1966; Liggett, 1994; Chanson, 2011). After the formation of the bore, there is an abrupt rise in water depth at the bore front that is a discontinuity in the water depth, and pressure and velocity fields. The arrival of the tidal bore is associated with some intense mixing and upstream advection of the suspended material (Branner, 1884; Tessier and Terwindt, 1994; Wolanski et al., 2001,2004). The tidal bore affected estuaries are the natural habitats, feeding zones and breeding grounds of several forms of fish species and aquatic life forms (Rulifson and Tull, 1999; Butcher, 2004; Chanson and Tan, 2010). The effects of tidal bores on sediment processes were studied previously (Chen et al., 1990; Tessier and Terwindt, 1994; Greb and Archer, 2007) and there are further anecdotal evidences. Past studies indicated that the arrival of the bore front was associated with intense bed material mixing and with upstream advection of suspended sediments. To date, the field observations of tidal bores remain very limited, and most studies were conducted with a coarse resolution in terms of temporal and spatial scales: it is challenging to analyse conclusively these data.

In the south-west of France, some large tidal bores are observed in the Gironde Estuary, and the Dordogne and Garonne Rivers (Fig. 1). The Garonne River is 575 km long excluding the Gironde Estuary and is affected by the tides from the confluence with the Dordogne River at Bec d'Ambès up to Castets. The tidal bore of the Garonne River occurs typically between Pont F. Mitterand in Bordeaux and upstream of Cadillac. In the present study, some detailed turbulence field measurements were conducted continuously at high-frequency (64 Hz) in the tidal bore of the Garonne River in Sept. 2010. The turbulent velocity components were sampled with an acoustic Doppler velocimeter (ADV) at 0.8 m beneath the free-surface. The tidal bore propagation was observed in the Garonne River on both 10 and 11 Sept. 2010. The results provided a unique characterisation of the turbulence and sediment flux close to the free-surface during the tidal bore events.

* Corresponding author.
E-mail address: h.chanson@uq.edu.au (H. Chanson).
URL: http://www.uq.edu.au/~e2hchans

0272-7714/$ – see front matter © 2011 Elsevier Ltd. All rights reserved.
doi:10.1016/j.ecss.2011.09.012

2. Study site and instrumentation

2.1. Presentation

The field study was conducted in the Garonne River (France) in the Bras d'Arcins (Arcins channel) between Île d'Arcins (Arcins Island) and the right bank close to Lastrene. The Arcins channel is about 1.8 km long, 70 m wide and about 1.1–2.5 m deep at low tide (Figs. 1 and 2). Fig. 1 shows a map of the Garonne River and Arcins channel, while Fig. 2 presents a cross-sectional survey conducted on 10 Sept. 2010 where z is the vertical elevation. In Fig. 2, the ADV sampling volume location and water level immediately prior to the bore are shown. The sampling site was selected because the tidal bore was well-developed across the Arcins channel width while access was facilitated to the banks at low water by a pontoon and ramp.

Although the tides are semi-diurnal, the tidal cycles have slightly different periods and amplitudes indicating some diurnal inequality (Fig. 3). Fig. 3 presents the water elevation observations recorded at Bordeaux about 9 km downstream of the sampling location and they are compared with the water elevations recorded on-site prior to and shortly after the passage of the tidal bore on the afternoons of the 10 and 11 Sept. 2010.

The field measurements were conducted under spring tidal conditions and the tidal range data are summarised in Table 1 (column 2). The measurements were conducted during the afternoon flood tides, and the sampling was stopped at sunset. The water elevations and some continuous high-frequency turbulence data were recorded prior to, during and after the passage of the tidal bore for a few hours each day. The start and end times are listed in Table 1 (columns 6 and 8). Further details and information were reported by Chanson et al. (2010).

2.2. Instrumentation

The free-surface elevations were measured manually using a survey staff. During the passage of the tidal bore, a video camera recorded the water level and the data were collected frame by frame at 25 fps. The survey staff was mounted 1 m beside the ADV unit towards the right bank, to minimise any interference with the ADV sampling volume.

Fig. 1. Map of the Garonne River and sampling site location.

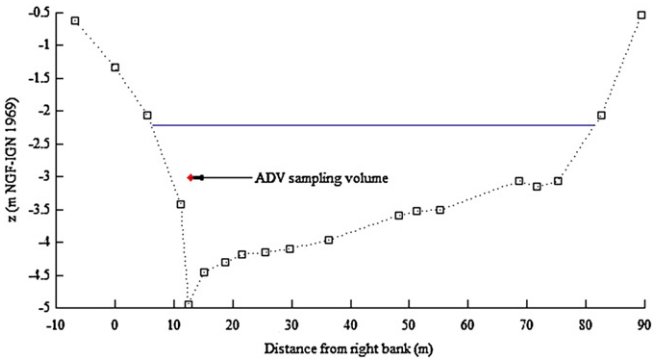

Fig. 2. Surveyed cross-section of Arcins channel with the low tide water level on 10 Sept. 2010 afternoon (blue line) and the corresponding ADV sampling volume location (red diamond) – looking upstream. (For interpretation of the references to colour in this figure legend, the reader is referred to the web version of this article.)

The turbulent velocities were measured with a Nortek™ Vector ADV (6 MHz, serial number VEC3332). The ADV system was equipped with a 3D downlooking head (Head ID VEC4665) and the unit was self-logging. The system was fixed to a heavy, sturdy pontoon and mounted vertically and the positive direction head was pointing downstream. The probe sampling volume was about 0.8 m below the free-surface (Table 1, column 9). Hence the present study was a point measurement that was probably not representative of the entire channel cross-section.

All the ADV data underwent a thorough post-processing procedure to eliminate any erroneous or corrupted data from the data sets to be analysed. The post-processing included the removal of communication errors, the removal of average signal to noise ratio data less than 15 dB and the removal of average correlation values less than 60% (McLelland and Nicholas, 2000). In addition, the phase-space thresholding technique developed by Goring and Nikora (2002) was applied to remove spurious points.

Further observations were recorded with a digital camera Pentax™ K-7, a digital video camera Canon™ MV500i, a digital video camera JVC™ GR-D225E and a HD digital video camera Canon™ HF10E.

2.3. Practical issues

The accuracy on the ADV velocity measurements was 1% of the velocity range (±2 m/s) (Nortek, 2005). The accuracy of the water

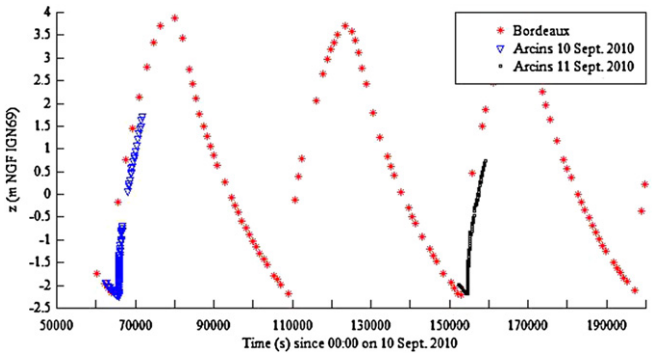

Fig. 3. Measured water elevations at Bordeaux (44°52′N, 0°33′W) (data: Vigicrue, Ministère de l'Environnement et du Développement Durable) and observations in the Arcins channel on 10 and 11 Sept. 2010.

Table 1
Tidal bore field measurements in the Arcins channel, Garonne River (France).

Date	Tidal range (m)	ADV system	Sampling rate (Hz)	Sampling duration	Start time	Tidal bore time	End time	Sampling volume
10/09/2010	6.03	Nortek Vector (6 MHz)	64	2 h 45 min	17:15	18:17	20:00	About 7 m from right bank waterline (at low tide), 0.81 m below water surface.
11/09/2010	5.89	Nortek Vector (6 MHz)	64	2 h 20 min	18:00	18:59	20:10	About 7 m from right bank waterline (at low tide), 0.81 m below water surface.

Notes: tidal range: measured at Bordeaux; all times are in French local times (GMT + 1).

elevation was 0.5 cm prior to the tidal bore and 1–2 cm during the tidal bore passage.

Note that the sampling duration was limited by installation of the ADV in the early afternoons and its dismantling at sunset.

On 10 Sept. 2010, the ADV was setup with a control volume size of 3.5 mm. The pressure, signal amplitude, SNR and backscatter data appeared correct, but the velocity components exhibited some unacceptable noise for frequencies larger than 0.02–0.1 Hz (Chanson et al., 2010). While the exact cause of the problem remained unknown, it was thought that the ADV system was overloaded with the small control volume.

Following some additional tests, a slightly different setup was selected on 11 Sept. 2010 with a 6.6 mm control volume size. The change yielded good quality data sets which included the turbulent velocity components.

3. Observations

The tidal bore propagation in the Arcins channel was similar on both days during the afternoons. (The morning bores took place in the darkness and were not investigated for safety.) The tidal bore formed first at the downstream end of the channel about 4 min 45 s before it reached the sampling location (Fig. 4A). The tidal bore expanded rapidly across the entire channel width as a breaking bore (Fig. 4B). As the bore propagated upstream, its shape evolved in response to the local bathymetry. About 200 m downstream of the sampling point, the bore became undular and its front was flatter (Fig. 4C). The tidal bore was undular as it passed in front of the sampling location, and the bore front was well marked as illustrated by the surfer riding ahead of the first wave crest in Fig. 4C and D. The undular tidal bore continued to propagate up to the upstream end of the channel for another 4 min. Fig. 4A–D shows the development of the tidal bore at the channel downstream end as well as its upstream propagation towards and past the sampling location.

The passage of the tidal bore was followed by a pseudo-chaotic wave motion lasting for several minutes after the bore. At the sampling location, the free-surface elevation rose very rapidly by 0.50 m and 0.41 m in the first 5 s on 10 and 11 Sept. 2010 respectively. For the next 35 min, the water elevation rose further by 1.69 m and 1.59 m on 10 and 11 Sept. 2010 respectively. Figs. 5A and 6 present the time-variations of the water depth at the ADV sampling location. Fig. 5A illustrates the rapid water level rise associated with the tidal bore passage, and the horizontal axis scale correspond to 60 s. Fig. 6 presents the water level variations during 1 h 23 min on both days.

The strength of a tidal bore is basically characterised by its Froude number. In the irregular channel, the bore Froude number Fr_1 is calculated as:

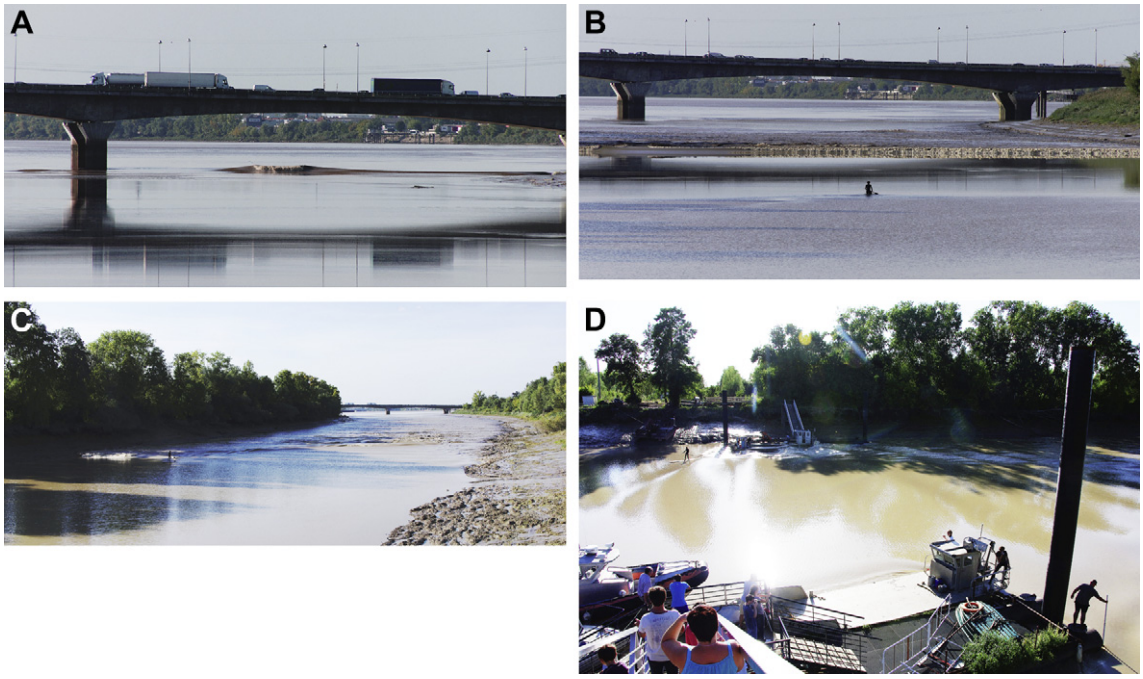

Fig. 4. Tidal bore in Bras d'Arcins (Arcins channel) on 10 Sept. 2010. (A) Tidal bore formation at the channel downstream end at 18:13:00 just upstream of Pont F. Mitterrand. (B) Breaking tidal bore at 18:15:14 – note the surfer awaiting the bore. (C) Undular tidal bore downstream of the sampling location at 18:17:18 – note surfer close to the Arcins Island. (D) Undular tidal bore shortly after passing the ADV sampling location (bottom right) at 18:17:42.

$$\mathrm{Fr}_1 = \frac{V_1 + U}{\sqrt{g \times \frac{A_1}{B_1}}} \quad \text{Irregular channel} \tag{1}$$

where V_1 is the initial flow velocity positive downstream, U is the bore celerity positive upstream, A_1 is the initial flow cross-section and B_1 is the initial free-surface width (Liggett, 1994; Chanson et al., 2010). The observed channel properties and bore celerity are summarised in Table 2. Equation (1) yields $\mathrm{Fr}_1 = 1.30$ and 1.20 for the field observations on 10 and 11 Sept. 2010 respectively. These values were typical of an undular tidal bore (Henderson, 1966; Chanson, 2011).

The turbulent velocity components on 11 Sept. 2010 are presented in Fig. 5, where V_x is the longitudinal velocity positive downstream, V_y is the horizontal transverse velocity positive towards the Arcins Island and V_z is the vertical velocity component positive upwards. The time-variations of the water depth at the survey staff are shown also. The longitudinal velocity data were checked qualitatively with some free-surface velocity observations of floating debris on the channel centreline and close to the right bank between the pontoon and the right bank (Chanson et al., 2010). The turbulent velocity data showed the marked effect of the passage of the bore front at $t = 68{,}302$ s (Fig. 5). The longitudinal velocity component highlighted some rapid flow deceleration during the passage of the bore front. As the bore front reached the sampling volume ($t = 68{,}302$ s), a sudden rise in the free-surface elevation took place associated with a sharp decrease in longitudinal velocity component and a flow reversal (Fig. 5A). The tidal bore passage was further characterised by some large fluctuations

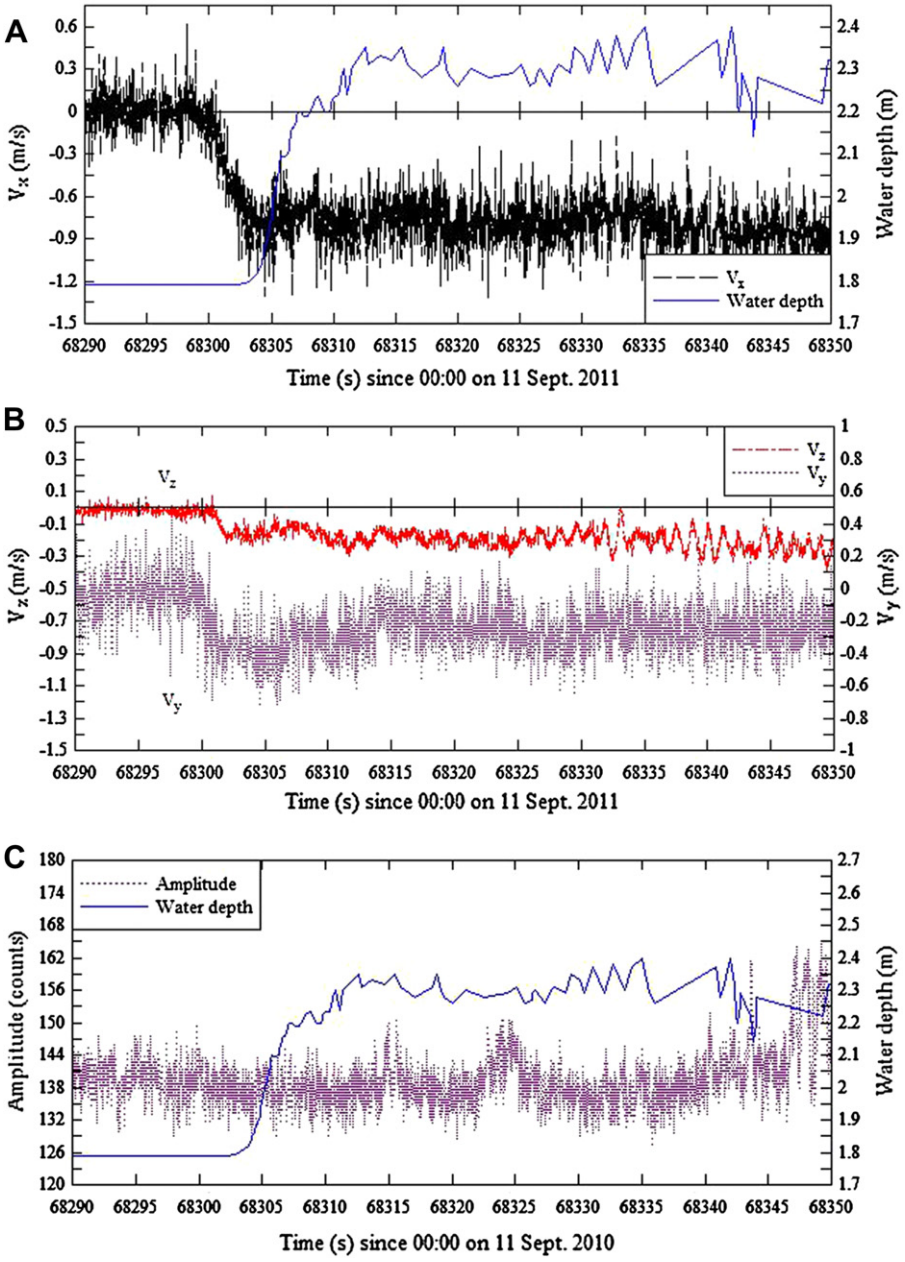

Fig. 5. Water depth, turbulent velocity components and amplitude at 0.8 m below the water surface during the tidal bore passage on 11 Sept. 2010 – post-processed ADV data, sampling rate: 64 Hz. (A) Water depth and horizontal velocity component V_x. (B) Transverse and vertical velocity components (V_y, V_z). (C) Signal amplitude (Ampl) and water depth.

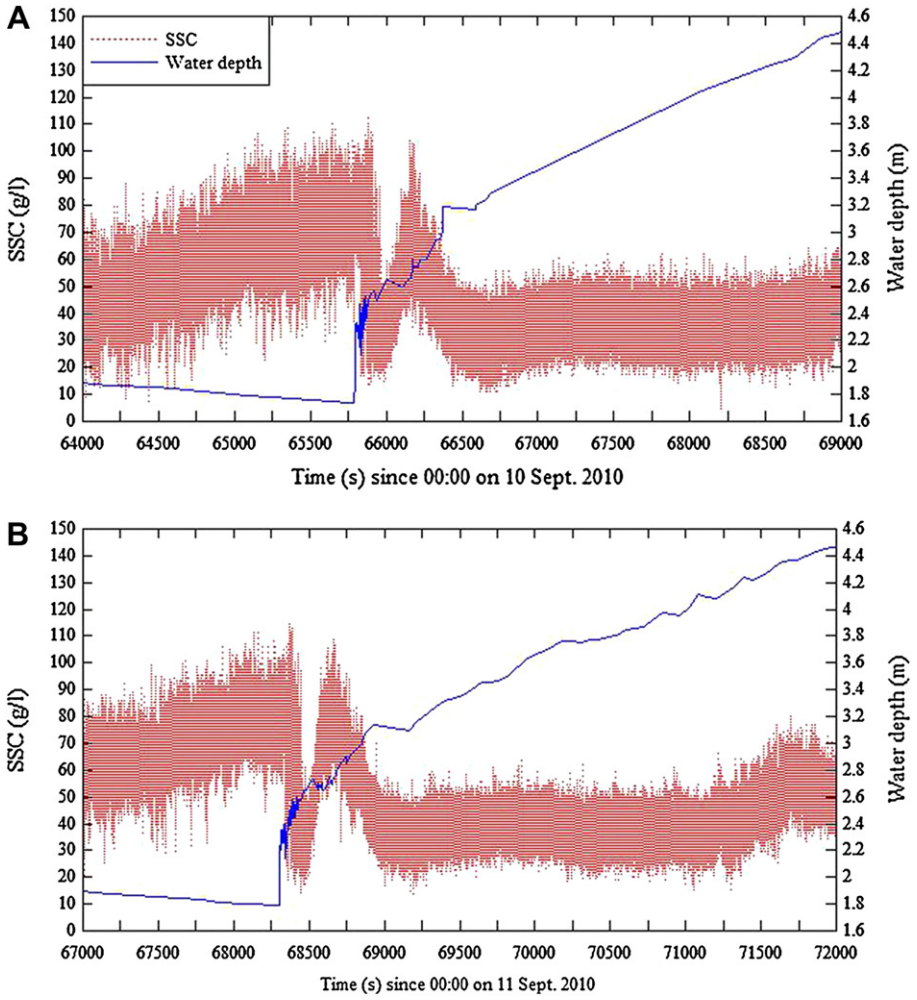

Fig. 6. Water depth and suspended sediment concentrations at 0.8 m below the water surface on 10 and 11 Sept. 2010 Post-processed ADV data, sampling rate: 64 Hz. (A) 10 Sept. 2010. (B) 11 Sept. 2010.

of all three turbulent velocity components. The observations were consistent with the earlier results of Wolanski et al. (2004) and Simpson et al. (2004) in the field, and Hornung et al. (1995), Koch and Chanson (2009) and Chanson (2010) in laboratory.

The longitudinal flow component changed from +0.3 m/s (oriented downriver) to −1 m/s (oriented upriver) immediately after the passage of the bore (Fig. 5A), with velocity fluctuations between 0 and −2 m/s for the entire study period. The large velocity fluctuations lasted for the entire sampling duration. The longitudinal velocity results were consistent with the visual observations before and after the tidal bore passage, although the surface current was stronger on the channel centreline than close to the right bank. At times, the authors noted some recirculation patterns next the waterline mark on the right bank, where the surface velocity flowed then downstream against the main flood flow direction.

After the passage of the bore, the transverse velocity data fluctuated between +0.6 and −1.1 m/s for the entire study period, and the time-averaged transverse velocity component was −0.28 m/s (Fig. 5B). The finding implied some net transverse circulation towards the right bank next to the free-surface. This flow pattern was linked possibly with the irregular channel cross-section and the existence of some secondary flow motion. The vertical velocity data highlighted a marked effect of the tidal bore. After the bore passage, the vertical velocity fluctuated between +0.1 and −0.8 m/s for the entire record, with a time-averaged value of about −0.28 m/s (Fig. 5B). The backscatter amplitude data are shown also in Fig. 5C.

Note that the ADV sampling volume depth ranged from 0.7 m to 0.9 m for the entire study duration, with an average of 0.8 m. The velocity data characterised therefore the turbulence in the upper water column. Further the ADV was fixed to a pontoon. Although heavy and sturdy, the vertical motion of the pontoon cannot be ignored.

Table 2
Tidal bore properties in the Arcins channel (Garonne River, France).

Date	V_1 (m/s)	U (m/s)	A_1 (m^2)	B_1 (m)	A_1/B_1 (m)	Fr_1	Remarks
10/09/2010	+0.33	4.5	106	75.4	1.40	1.30	Undular bore.
11/09/2010	+0.30	4.2	109	75.8	1.43	1.20	Undular bore.

Notes: A_1: channel cross-section area immediately prior to the bore passage; B_1: free-surface width immediately prior to the bore passage; Fr_1: tidal bore Froude number (equation (1)); U: tidal bore celerity positive upstream on the channel centreline; V_1: downstream surface velocity on the channel centreline immediately prior to the bore passage.

4. Sediment properties

The Garonne River bed material was documented by collecting some samples just above the low water mark at low tide on 11 Sept. 2010 next to the measurement site. The bed material was

a cohesive mud mixture consisting of fine mud and silt materials, although the granulometry was not tested. It could be considered as a form of mud cream (*crème de vase*). A series of laboratory tests were conducted to characterise the bed material properties.

The density of the wet sediment was $s = 1.418$. The rheological properties of mud samples were tested with a Rheometer TA-ARG2 (Serial 5L2980) equipped with a plane-cone setup ($\varnothing = 60$ mm, cone angle: 20.005°) and a gap truncation of 52 μm. Between the sample collection and the tests, the mud was left to consolidate for 3 days. Each specimen was subjected to a controlled strain rate loading and unloading between 0.01 s^{-1} and 1000 s^{-1} with steady state flow steps s at constant temperature (20 °C). The rheometry tests provided some information on the apparent yield stress of the fluid τ_c and the effective viscosity μ. The yield stress and apparent viscosity were estimated during the unloading phase, to be consistent with earlier thixotropic experiments (Roussel et al., 2004; Chanson et al., 2006). The yield stress and viscosity results were derived by fitting the rheometer data with a Herschel–Bulkley model between shear stress τ and shear rate $\partial V/\partial z$:

$$\tau = \tau_c + \mu \times \left(\frac{\partial V}{\partial z}\right)^m \quad (2)$$

where $0 < m \leq 1$ (Huang and Garcia, 1998; Wilson and Burgess, 1998).

Some typical experimental results are presented in Fig. 7. The behaviour of the mud material was fairly typical of a thixotropic material and the data highlighted some differences between the loading and unloading sequence. The magnitude of the shear rate during unloading was smaller than the shear rate magnitude during loading for a given shear stress. For shear rates larger than 300 s^{-1}, the tests gave close results, suggesting a conservation of the macroscopic structure possibly in the form of particle arrangement into thin layers. On average over the tests, the apparent viscosity was $\mu = 48.8$ Pa s, the yield stress was about $\tau_c = 55.5$ Pa and m ~ 0.275.

The acoustic Doppler velocimeter (ADV) was calibrated in terms of suspended sediment concentration. While the ADV is designed to record the instantaneous velocity components, the signal strength, or acoustic backscatter strength, may be related to the instantaneous suspended sediment concentration (SSC) with proper calibration (Kawanisi and Yokosi, 1997; Fugate and Friedrichs, 2002). Although the method was initially developed for non-cohesive sediments, it was recently extended successfully to cohesive materials (Chanson et al., 2008; Ha et al., 2009). The calibration of the ADV was accomplished by measuring the signal amplitude of known, artificially produced concentrations of material obtained from the bed material sample, diluted in tap water and thoroughly mixed. The suspended sediment concentrations ranged from less than 0.02 g/l to 74 g/l, and all the experiments were conducted within a couple of days from the sample collection. The laboratory experiments were conducted with the same Nortek™ Vector ADV unit using the same settings as for the field observations. For each test, a known mass of sediment was introduced in a water tank which was continuously stirred with two propeller mixers. In addition the tank was stirred manually during the most turbid water tests to check and prevent any sediment deposition on the tank bottom. The mass of wet sediment was measured with a Mettler™ Type PM200 (Serial G77187) balance, and the error was less than 0.01 g. The mass concentration was deduced from the measured mass of wet sediment and the measured water tank volume.

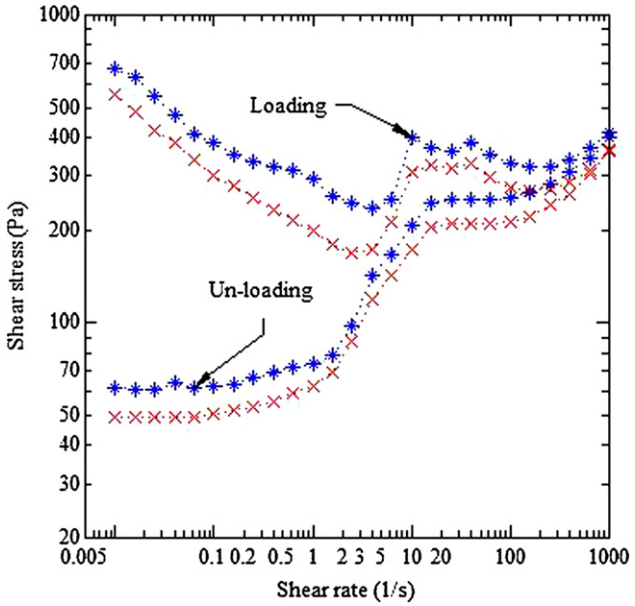

Fig. 7. Rheometry tests: loading and unloading cycle of mud samples.

The relationships between acoustic backscatter amplitude (Ampl), acoustic backscatter intensity (BSI) and suspended sediment concentrations (SSC) were tested systematically, and the experimental results are summarised in Fig. 8. Herein the backscatter intensity was deduced from the average amplitude as:

$$\text{BSI} = 10^{-5} \times 10^{0.043 \times \text{Ampl}} \quad (3)$$

where BSI is dimensionless and the average amplitude Ampl is in counts. The coefficient 10^{-5} is a value introduced to avoid large values of backscatter intensity (Nikora and Goring, 2002). First the results were independent of the ADV settings. No major difference was observed between the calibration tests from the ADV settings on 10 and 11 Sept. 2010. Second there was a good correlation between all the data showing two characteristic trends. For SSC ≤ 0.48 g/l, the data yielded a monotonic increase in suspended sediment concentration with increasing backscatter intensity. The relationships between SSC and amplitude, and SSC and BSI, were roughly linear. For larger SSCs (i.e. SSC > 0.48 g/l), the experimental results demonstrated a decreasing backscatter intensity with increasing SSC. For the laboratory tests with low suspended loads (SSC ≤ 0.48 g/l), the best-fit relationships were:

$$\text{SSC} = 0.0367 \times \text{Ampl} - 6.02 \quad \text{SSC} \leq 0.48 \text{ g/l} \quad (4a)$$

$$\text{SSC} = 0.0019 \times \text{BSI} - 0.189 \quad \text{SSC} \leq 0.48 \text{ g/l} \quad (4b)$$

where the suspended sediment concentration SSC is in g/l, and the amplitude Ampl is in counts. For large suspended sediment loads (i.e. SSC > 0.48 g/l), the data were best correlated by

$$\text{SSC} = 381.7 - 2.17 \times \text{Ampl} \quad \text{SSC} > 0.48 \text{ g/l} \quad (5a)$$

$$\text{SSC} = 79.15 \times \exp(-0.010 \times \text{BSI}) \quad \text{SSC} > 0.48 \text{ g/l} \quad (5b)$$

Equations (4a), (4b) and (5a), (5b) are compared with the data in Fig. 8. For large suspended sediment concentration within 0.4 < SSC < 75 g/l, the results showed a good correlation between the acoustic backscatter strength and the SSC, although the ADV signal was saturated.

During the present field investigations, the authors observed that the Arcins channel waters were very turbid before, during and after the tidal bore. For example, they could not see their fingers below 1–3 cm from the water surface, and the people who went

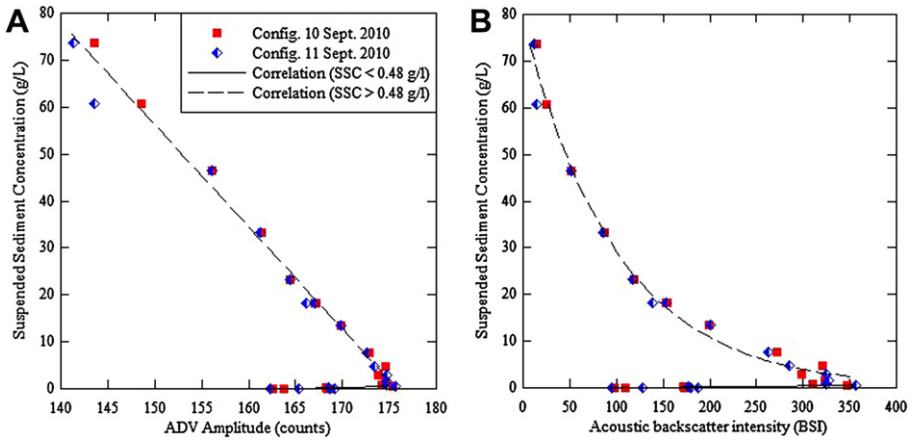

Fig. 8. Relationship between suspended sediment concentration, acoustic signal amplitude and acoustic backscatter intensity with the sediment mud collected at Arcins – comparison between the data and equations (4a), (4b) and (5a), (5b). (A) Relationship between suspended sediment concentration (SSC in g/l) and acoustic signal. (B) Relationship between suspended sediment concentration (SSC in g/l) and acoustic backscatter intensity (BSI).

into the water got covered by fine sediment materials. In the Gironde Estuary and Garonne River estuarine zone, the currents exceed the critical erosion except during neap tides (Cancino and Neves, 1999). Recent SSC observations reported typically values from 0.5 g/l to 2.5 g/l close to the surface (Doxaran et al., 2009). Therefore equations (5a) and (5b) were considered to be representative of the relationship between the suspended sediment concentration (SSC) and the acoustic backscatter intensity (BSI) in the Arcins channel on 10 and 11 Sept. 2010.

5. Suspended sediment concentrations and fluxes

The visual observations prior, during and after the tidal bore showed a significant amount of suspended sediment load in the waters. The waters were very turbid and murky. Further a large number of turbulent patches of mud flocs were seen at the free-surface during the flood flow for the 2 h after the tidal bore. These turbulent patches were likely the results of turbulent burst events, generated next to the bed associated with coherent flow structures or macroturbulence (Nezu and Nakagawa, 1993; Trevethan and Chanson, 2010). Bursting is the quasi-cyclic turbulent energy production in turbulent boundary layers first identified by Kline et al. (1967) playing a major role in terms of sediment scour, transport and accretion. In natural systems, a number of studies linked the origin of the macroturbulence to shear layer development in the wake of bed forms, and the re-suspension of bottom sediment materials (Barua and Rahman, 1998; Best, 2005).

The time-variations of the suspended sediment concentration (SSC) deduced from equations (5a) and (5b) are presented in Fig. 6A and B for the field studies on 10 and 11 Sept. 2010 respectively. The water depth data are reported also for completeness, as the ADV apparatus was fixed to the floating pontoon. Both data sets were near-identical (Fig. 6). They showed some increase in SSC with decreasing water depth prior to the tidal bore arrival. The trend could be linked with the larger depth-averaged shear stress in the shallower water column as well as some more intense secondary motion at the end of the ebb tide. The pontoon went down with the decreasing water depth, as well as the sampling volume of the ADV fixed to the structure. When the tidal bore front reached the measurement zone, the water depth suddenly increased from 1.8 m to 2.25 m, the SSC increased with time although the ADV elevation increased. Importantly the maximum SSC did not coincide with the exact moment of the bore front passage. The constant increase of SSC was thus associated with the high turbulent intensity, a vertical flux of sediment suspension and the strong mixing capacity of the tidal bore front. The tidal bore was associated with large fluctuations of the SSC including during the flood flow motion. Some unusual event was observed about 100 s after the tidal bore front on both days, lasting for more than 10 min (e.g. $t = 68{,}400$–$69{,}000$ s in Fig. 6B). On both days, the event details indicated a sharp decrease in SSC about 50–70 s after the bore front passage (e.g. $t = 68{,}355$ s in Fig. 6B), followed by a major event with large and rapid fluctuations in SSC: e.g., between $t = 68{,}380$ and 68,800 s in Fig. 6B. It is conceivable that the bed material was sheared during the tidal bore front passage and associated flow reversal, and the sediments were convected upwards by the flood tide turbulent motion. The suspended sediment would be advected upstream behind the bore and reach the free-surface with some delay after the front passage.

After the bore front passage, the water depth increased with time as the river flowed upstream, and the ADV sampling volume rose away from the river bed. The decrease in SSC could be associated with a lesser amount of suspended sediment reaching the ADV sampling volume. The sedimentation of the heaviest particles could have also been more important than the re-suspension. This was followed by a major event with large and rapid fluctuations in SSC: e.g., between $t = 68{,}380$ and 68,800 s in Fig. 6B. The drastic increase of concentration could be caused by the volumes of mud cream from the river banks affected by the water level rise. It could have also resulted from the nature of the suspensions, as the mud cream trapped on the river banks could release more small-sized suspensions with some delay. It could also be due to the chaotic motion of the flow. At the end of ebb tide, the river bank mud was in contact with air, and the sediment matter flocked and dried up. After the tidal bore induced motion, the sediment flocks sediment could have been disintegrated and a greater particle counts have been recorded in the ADV sampling volume, showing possibly higher SSCs. Finally, during the flood flow, the water depth increased with time although, the SSC remained constant on average. It seemed that a pseudo-stationary phase was reached next to the free-surface. Sediments must be sufficiently and permanently mixed over the whole water column to get a constant concentration value, in particular near the free-surface where the ADV sampling volume was located. As already described, large dynamic turbulent patches were observed, bursting from below the free-surface and stretching it, creating some large circles of different brown colours. This was the sign that a large amount of sediment was brought to the surface and mixed.

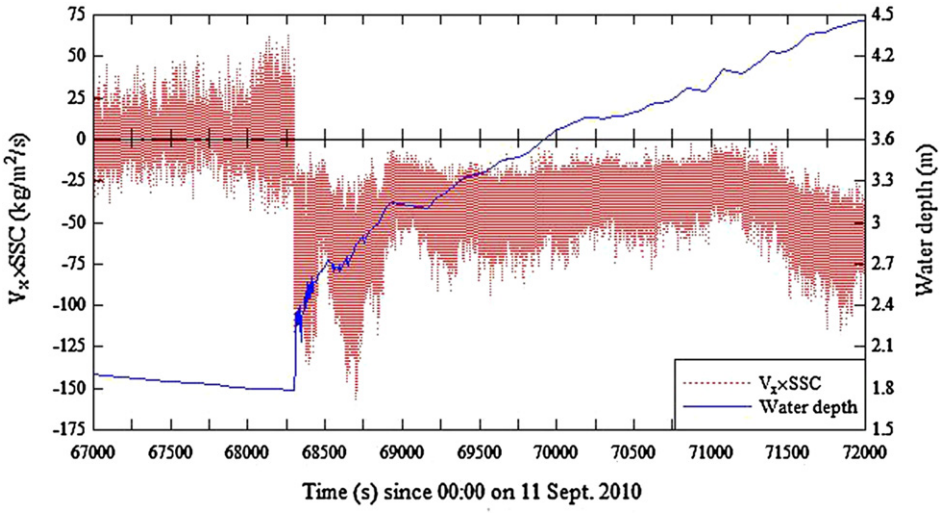

Fig. 9. Time-variations of the suspended sediment flux per unit area (SSC × V_x) at 0.8 m below the surface and water depth on 11 Sept. 2010 – post-processed ADV data, sampling rate: 64 Hz.

The present results were used to estimate the instantaneous advective suspended sediment flux per unit area q_s calculated as:

$$q_s = \mathrm{SSC} \times V_x \tag{6}$$

where q_s and V_x are positive in the downstream direction. In equation (6), the suspended sediment concentration SSC is in kg/m^3, the longitudinal velocity component V_x is in m/s and the sediment flux per unit area is in kg/m^2/s. The results are presented in Fig. 9 in terms of the instantaneous sediment flux q_s. The sediment flux data showed typically a downstream positive suspended sediment flux during the end of the ebb tide prior to the tidal bore (Fig. 9). The arrival of the tidal bore was characterised by a rapid reversal and the suspended sediment flux was negative during the flood tide after the tidal bore passage. The instantaneous sediment flux data q_s showed some large and rapid time-fluctuations that derived from a combination of velocity and suspended sediment concentration fluctuations. The suspended sediment flux data demonstrated some high-frequency fluctuations with some form of sediment flux bursts that were likely linked to and caused by some turbulent bursting phenomena next to the boundaries. Some low-frequency fluctuations in sediment flux were also observed (Fig. 9).

For the study, the sediment flux data were integrated with respect of time. The result gives the net sediment mass transfer per unit area during a period T:

$$\int_T \mathrm{SSC} \times V_x \times \mathrm{d}t \tag{7}$$

Prior the tidal bore ($65{,}000 < t < 68{,}200$ s), the net sediment mass transfer per area was positive and equation (7) yielded $+4770$ kg/m^2 during the 53 min of data prior the tidal bore. Immediately after the passage of the bore, the net sediment mass transfer per unit area was negative and equal to 186,120 kg/m^2 for $68{,}300 < t < 72{,}500$ s (i.e. 70 min). That is, the net sediment flux was about 30 times larger in magnitude than the sediment flux prior to the tidal bore. Past studies indicated that the arrival of the bore front was associated with intense bed material mixing and with upstream advection of suspended material behind the bore front (Chen et al., 1990; Greb and Archer, 2007). The present data set (Fig. 9) supported and complemented the findings.

6. Conclusion

Some detailed turbulent velocity measurements were conducted continuously at high-frequency (64 Hz) prior to, during and after the tidal bore of the Garonne River (France) in Sept. 2010. The velocity components were sampled with an acoustic Doppler velocimeter (ADV) with its sampling volume about 0.8 m beneath the free-surface in the Arcins channel.

The tidal bore was undular. Its Froude number was estimated from the channel bathymetry and tidal bore observations: $\mathrm{Fr}_1 = 1.30$ and 1.20 on 10 and 11 Sept. 2010 respectively. The bore passage was characterised by a pseudo-chaotic wave motion lasting for several minutes after the bore. The free-surface elevation rose very rapidly by 0.50 m and 0.41 m in the first 5 s, and by further 1.69 m and 1.59 m for the next 35 min on 10 and 11 Sept. 2010 respectively. The turbulent velocity data showed the marked impact of the tidal bore propagation. The longitudinal velocity component highlighted some rapid flow deceleration during the passage of the tidal bore, associated with a sudden rise in the free-surface elevation, and a flow reversal after the tidal bore front passage. The observations were consistent with earlier field and laboratory results, and they demonstrated the intense turbulent mixing induced by the tidal bore.

The ADV backscatter amplitude was calibrated in terms of the suspended sediment concentration in laboratory using the soft mud bed material. The results provided a unique characterisation of the turbulence, suspended sediment concentration (SSC) and sediment flux beneath to the free-surface during the tidal bore with high temporal and spatial resolution. The tidal bore passage was associated with large fluctuations in SSC, and some high SSC level was observed about 100 s after the tidal bore front lasting for more than 10 min. It is thought that the turbulent mixing induced by the tidal bore passage convected upwards the bed material and the suspended sediments were advected upstream behind the bore, reaching the free-surface with some delay after the front passage. While, prior to the tidal bore, the suspended sediment flux data showed a downstream motion, the arrival of the tidal bore was characterised by a rapid sediment flux reversal. The magnitude of net sediment mass transfer per area was 30 times larger than the ebb tide net flux and it was directed upstream.

A striking feature of the analysed data set was the large and rapid fluctuations in suspended sediment flux during the tidal bore

and flood flow. This feature was not documented, but an important difference between the ADV data set used in this study from earlier reported field measurements was that the present data were collected continuously at relatively high-frequency (64 Hz) during a relatively long period (at least 2 h). It is however acknowledged that the present investigation was a point measurement about 0.8 m beneath the free-surface. Any extrapolation would imply that the sampling volume was representative of the entire channel cross-section.

Lastly the present field study was conducted at the end of the summer during low freshwater conditions. Both spring tide conditions and low water levels were essential for the occurrence of the tidal bore of the Garonne River in the Arcins channel. During the wet winter season, on the other hand, the tidal bore is unseen when the river water level is higher, even during spring tides.

Acknowledgements

The authors thank all the people who participated to the field works. They acknowledge the assistance of Patrice and the permission to access and use the pontoon in the Bras d'Arcins. The ADV was provided kindly by Dr Dominique Mouazé (University of Caen, France). Hubert Chanson acknowledges some financial assistance from the Université de Bordeaux and the University of Queensland. Bruno Simon acknowledges a joint scholarship funded by the TREFLE Laboratory and the Région Aquitaine. The financial assistance of the Agence Nationale de la Recherche (Projet MASCARET 10-BLAN-0911-01) is acknowledged.

References

Barua, D.K., Rahman, K.H., 1998. Some aspects of turbulent flow structure in large alluvial rivers. Journal of Hydraulic Research, IAHR 36 (3), 235–252.

Best, J., 2005. Kinematics, topology and significance of dune-related macroturbulence: some observations from the laboratory and field. In: Special Publication Int. Ass. Sediment, vol. 35, pp. 41–60.

Branner, J.C., 28 Nov. 1884. The pororoca, or bore, of the Amazon. Science 4 (95), 488–492, Also 1885, Rand, Avery & Co, Boston, USA, pp. 3–12. (Also 1903, List of Publications by Members of the Department of Geology, Stanford University, USA.).

Butcher, J.G., 2004. The closing of the frontier. A history of the marine fisheries of Southeast Asia c. 1850–2000. In: A Modern Economic History of Southeast Asia Series. KITLV Press, Leiden, The Netherlands. 442 pages.

Cancino, L., Neves, R., 1999. Hydrodynamic and sediment suspension modelling in estuarine systems. Part II: application to the Western Scheldt and Gironde Estuaries. Journal of Marine Systems 22, 117–131.

Chanson, H., 2010. Unsteady turbulence in tidal bores: effects of bed roughness. Journal of Waterway, Port, Coastal, and Ocean Engineering, ASCE 136 (5), 247–256. doi:10.1061/(ASCE)WW.1943-5460.0000048.

Chanson, H., 2011. Tidal Bores, Aegir, Eagre, Mascaret, Pororoca: Theory and Observations. World Scientific, Singapore, ISBN 9789814335416.

Chanson, H., Jarny, S., Coussot, P., 2006. Dam break wave of thixotropic fluid. Journal of Hydraulic Engineering, ASCE 132 (3), 280–293. doi:10.1061/(ASCE)0733-9429.

Chanson, H., Lubin, P., Simon, B., Reungoat, D., 2010. Turbulence and Sediment Processes in the Tidal Bore of the Garonne River: First Observations. Hydraulic Model Report No. CH79/10. School of Civil Engineering, The University of Queensland, Brisbane, Australia. 97 pages.

Chanson, H., Takeuchi, M., Trevethan, M., 2008. Using turbidity and acoustic backscatter intensity as surrogate measures of suspended sediment concentration in a small sub-tropical estuary. Journal of Environmental Management 86 (4), 1406–1416. doi:10.1016/j.jenvman.2007.07.009.

Chanson, H., Tan, K.K., 2010. Turbulent mixing of particles under tidal bores: an experimental analysis. Journal of Hydraulic Research, IAHR 48 (5), 641–649. doi:10.1080/00221686.2010.512779.

Chen, J., Liu, C., Zhang, C., Walker, H.J., 1990. Geomorphological development and sedimentation in Qiantang Estuary and Hangzhou Bay. Journal of Coastal Research 6 (3), 559–572.

Doxaran, D., Froidefond, J.M., Castaing, P., Babin, M., 2009. Dynamics of the turbidity in a macrotidal estuary (the Gironde, France): observations from field and MODIS satellite data. Estuarine, Coastal and Shelf Science 81, 321–332.

Fugate, D.C., Friedrichs, C.T., 2002. Determining Concentration and fall velocity of estuarine particle populations using ADV, OBS and LISST. Continental Shelf Research, vol. 22, 1867–1886.

Goring, D.G., Nikora, V.I., 2002. Despiking acoustic Doppler velocimeter data. Journal of Hydraulic Engineering, ASCE 128 (1), 117–126. discussion: 129 (6), 484–489.

Greb, S.F., Archer, A.W., 2007. Soft-sediment deformation produced by tides in a Meizoseismic Area, Turnagain Arm, Alaska. Geology 35 (5), 435–438.

Ha, H.K., Hsu, W.Y., Maa, J.P.Y., Shao, Y.Y., Holland, C.W., 2009. Using ADV backscatter strength for measuring suspended cohesive sediment concentration. Continental Shelf Research 29, 1310–1316.

Henderson, F.M., 1966. Open Channel Flow. MacMillan Company, New York, USA.

Hornung, H.G., Willert, C., Turner, S., 1995. The flow field downstream of a hydraulic jump. Journal of Fluid Mechanics 287, 299–316.

Huang, X., Garcia, M., 1998. A Herschel–Bulkley model for mud flow down a slope. Journal of Fluid Mechanics 374, 305–333.

Kawanisi, K., Yokosi, S., 1997. Characteristics of suspended sediment and turbulence in a tidal boundary layer. Estuarine, Coastal and Shelf Science 38, 447–469.

Kline, S.J., Reynolds, W.C., Schraub, F.A., Runstaller, P.W., 1967. The structure of turbulent boundary layers. Journal of Fluid Mechanics 30 (4), 741–773. doi:10.1017/S0022112067001740.

Koch, C., Chanson, H., 2009. Turbulence measurements in positive surges and bores. Journal of Hydraulic Research, IAHR 47 (1), 29–40. doi:10.3826/jhr.2009.2954.

Liggett, J.A., 1994. Fluid Mechanics. McGraw-Hill, New York, USA.

McLelland, S.J., Nicholas, A.P., 2000. A new method for evaluating errors in high-frequency ADV measurements. Hydrological Processes 14, 351–366.

Nezu, I., Nakagawa, H., 1993. Turbulence in open-channel flows. In: IAHR Monograph, IAHR Fluid Mechanics Section. Balkema Publ., Rotterdam, The Netherlands. 281 pages.

Nikora, V., Goring, D., 2002. Fluctuations of suspended sediment concentration and turbulent sediment fluxes in an open-channel flow. Journal of Hydraulic Engineering, ASCE 128 (2), 214–224.

Nortek, 2005. Vector Current Meter. User Manual Nortek AS, Revision H 86 pages.

Roussel, N., Le Roy, R., Coussot, P., 2004. Thixotropy modelling at local and macroscopic scales. Journal of Non-Newtonian Fluid Mechanics 117 (2–3), 85–95.

Rulifson, R.A., Tull, K.A., 1999. Striped bass spawning in a tidal bore river: the Shubenacadie Estuary, Atlantic Canada. Transactions of the American Fisheries Society 128, 613–624.

Simpson, J.H., Fisher, N.R., Wiles, P., 2004. Reynolds stress and TKE production in an estuary with a tidal bore. Estuarine, Coastal and Shelf Science 60 (4), 619–627.

Tessier, B., Terwindt, J.H.J., 1994. An example of soft-sediment deformations in an intertidal environment – the effect of a tidal bore. Comptes-Rendus de l'Académie des Sciences, Série II 319 (2), 217–233. Part 2 (in French).

Trevethan, M., Chanson, H., 2010. Turbulence and turbulent flux events in a small estuary. Environmental Fluid Mechanics 10 (3), 345–368. doi:10.1007/s10652-009-9134-7.

Wilson, S.D.R., Burgess, S.L., 1998. The steady, spreading flow of a rivulet of mud. Journal of Non-Newtonian Fluid Mechanics 79, 77–85.

Wolanski, E., Moore, K., Spagnol, S., D'Adamo, N., Pattieratchi, C., 2001. Rapid, human-induced siltation of the macro-tidal Ord River Estuary, Western Australia. Estuarine, Coastal and Shelf Science 53, 717–732.

Wolanski, E., Williams, D., Spagnol, S., Chanson, H., 2004. Undular tidal bore dynamics in the Daly Estuary, Northern Australia. Estuarine, Coastal and Shelf Science 60 (4), 629–636.